

Interpretation of Doppler Weather Radar Displays of Midlatitude Mesoscale Convective Systems

Robert A. Houze, Jr.,*
S. A. Rutledge,[†]
M. I. Biggerstaff,*
and B. F. Smull[‡]

Abstract

The utility of color displays of Doppler-radar data in revealing real-time kinematic information has been demonstrated in past studies, especially for extratropical cyclones and severe thunderstorms. Such displays can also indicate aspects of the circulation within a certain type of mesoscale convective system—the squall line with trailing “stratiform” rain. Displays from a single Doppler radar collected in two squall-line storms observed during the Oklahoma-Kansas PRE-STORM project conducted in May and June 1985 reveal mesoscale-flow patterns in the stratiform rain region of the squall line, such as front-to-rear storm-relative flow at upper levels, a subsiding storm-relative rear inflow at middle and low levels, and low-level divergent flow associated with strong mesoscale subsidence. “Dual-Doppler” analysis further illustrates these mesoscale-flow features and, in addition, shows the structure of the convective region within the squall line and a mesoscale vortex in the “stratiform” region trailing the line. A refined conceptual model of this type of mesoscale convective system is presented based on previous studies and observations reported here.

Recognition of “single-Doppler-radar” patterns of the type described in this paper, together with awareness of the conceptual model, should aid in the identification and interpretation of this type of mesoscale system at future NEXRAD sites. The dual-Doppler results presented here further indicate the utility of multiple-Doppler observations of mesoscale convective systems in the STORM program.

1. Introduction

During May and June of 1985 the Oklahoma-Kansas Preliminary Regional Experiment for Stormscale Operational and Research Meteorology—Central Phase (PRE-STORM) was conducted (Cunning 1986). This program focused on mesoscale convective systems (MCSs) as they migrated across the Great Plains.¹ These

storms are important in the United States because they are responsible for much of the warm-season rainfall and severe weather over the central portion of the country (Fritsch et al. 1986). They pose a significant forecasting problem because their characteristic time and space scales make them difficult to resolve, track, and predict with present operational observing networks. Typically, MCSs are hundreds of kilometers in total horizontal dimension at maturity, and have lifetimes on the order of 10 hours. Important substructures (convective cells and lines, gust fronts, mesolows and mesohighs, tornadoes, etc.) occur within the MCS on horizontal scales ranging from 1 to 50 km; the circulations associated with these features must also be resolved. The need to explore MCSs in more detail is one of the primary motivations for the National STORM Program (NCAR 1984).

PRE-STORM was designed as a precursor to larger projects to be undertaken as part of the National STORM Program. One objective of PRE-STORM was a preliminary scientific investigation of mechanisms important to the genesis, intensification, and dissipation of MCSs. A second broad objective was to determine optimal ways to deploy and operate new observational technology in the study of MCSs, both for future research investigations and for use in operational meteorology. Successful achievement of these scientific and observational objectives is expected to sharpen the goals of the National STORM Program and have a beneficial impact on operational forecasting.

One new technology used to study MCSs in PRE-STORM was a network of three wind profilers, deployed to test their capability to determine the three-dimensional kinematic structure of MCSs and their environs. Analyses of these data have been discussed by Augustine and Zipser (1987). As another component of PRE-STORM, two National Oceanic and Atmospheric Administration (NOAA) WP-3D aircraft, one carrying a 3-cm-wavelength Doppler radar, were routed through and around MCSs to evaluate the feasibility of collecting airborne microphysical and radar data in the study of this type of storm. Coordinated data collection was performed between the NOAA airborne Doppler radar and the ground-based Doppler radars to gain insight into the kinematic structure of the storms (Ray and Jorgensen 1988).

Two ground-based Doppler-radar networks were

* Department of Atmospheric Sciences, AK-40, University of Washington, Seattle, WA 98195.

[†] Department of Atmospheric Science, Colorado State University, Fort Collins, CO 80523.

[‡] National Oceanic and Atmospheric Administration, National Severe Storms Laboratory, Mesoscale Research Division, Boulder, CO 80303.

¹ We adopt the definition of *mesoscale convective system* used in the *National Storm Program: STORM-CENTRAL Phase* (NCAR, 1984): viz., a precipitation system that has a horizontal scale of 10–500 km and includes significant convection during some part of its lifetime. The MCSs include the mesoscale convective complexes described by Maddox (1980), as well as other squall lines and groups of convective storms.

used in PRE-STORM. One network was located in central Oklahoma and consisted of the two 10-cm-wavelength Doppler radars operated by the National Severe Storms Laboratory (NSSL). The second network was situated west of Wichita, Kansas, where two National Center for Atmospheric Research (NCAR) mobile 5-cm-wavelength Doppler radars (CP-3 and CP-4) were located. These networks collected both "single-Doppler" and coordinated "dual-Doppler" data throughout the eight-week field program.²

Both profilers and Doppler radar (the next-generation weather radar, or NEXRAD) facilities will be major new observational tools for the National Weather Service beginning in the early 1990s. The NEXRAD systems will be 10-cm Doppler radars with real-time color displays of "reflectivity" and "unfolded" velocity fields in plan-position indicator (PPI) mode (Ray and Colbert 1982).

With the placement of NEXRAD radars in the central portion of the United States, MCSs will be probed routinely by Doppler radar. Operational meteorologists will be able to view the kinematic and precipitation structure of these storms in real time, thus facilitating analyses and forecasts of wind, precipitation amounts, and other storm features. Careful inspection of the color display of a single Doppler radar, together with good conceptual models, can provide timely information regarding the kinematics and structures of the MCSs.

Several studies have previously shown the utility of real-time color displays from a Doppler radar in revealing the airflows and precipitation characteristics of a variety of storm types and events. Real-time single-Doppler displays of wind patterns in extratropical cyclones were described by Baynton et al. (1977). Matejka and Hobbs (1981) discussed the utility of these displays in nowcasting frontal-precipitation patterns. Ray et al. (1980) described the color display of radial velocity in tornadic thunderstorms, and Wilson et al. (1980) presented displays for a variety of phenomena, including widespread precipitation, gust fronts, downbursts, and tornadoes, as well as displays of airflow in the clear-air boundary layer. None of these studies, however, have shown how the single-Doppler data are able to indicate the presence of mesoscale circulation features within MCSs.

² During single-Doppler data collection, at least one of the radars would collect data over a set of 360° azimuthal sweeps using a sequence of planned-position indicators (PPIs) with increasingly higher elevation angles. This provided as large a Doppler-radar view of the storm as possible. During dual-Doppler data collection, the radars were operated in coordination with each other to collect data over a smaller region with higher temporal and spatial resolution. The region over which the higher resolution data were collected was the region in which a multiple-Doppler analysis (dual-Doppler analysis in this case) could be performed to determine both components of the horizontal wind.

Real-time single-Doppler-radar data can also be used to reveal mesoscale flow patterns in a characteristic type of MCS documented in PRE-STORM—the squall line with trailing stratiform precipitation.³ A conceptual model of this type of storm is presented to aid in the interpretation of the single-Doppler-radar data.

2. Conceptual model

The type of MCS we considered here was identified in middle latitudes by Newton (1950), Fujita (1955), and Pedgley (1962). At about the same time, rather similar squall lines with trailing regions of stratiform rain were identified in the tropics (Hamilton and Archbold 1945; Zipser 1969). Although there are some differences between tropical and midlatitude squall lines, the broad mesoscale airflow features that we identify for midlatitude systems can be considered fairly representative of tropical cases as well.

The conceptual model in a vertical cross section (oriented perpendicular to the line of convective clouds) through a squall line with a trailing stratiform-precipitation region is shown in figure 1. The heavy black line in figure 1 indicates the boundary of the storm as seen by a weather radar. The light scalloped line indicates the horizontal and vertical extent of the clouds as determined from aircraft and satellite observations. The stippling indicates regions of enhanced radar reflectivity.⁴ This model is based on previous conceptual models of both midlatitude and tropical systems presented by Newton (1950), Fujita (1955), Pedgley (1962), Zipser (1969, 1977), Houze (1977), Gamache and Houze (1982), Smull and Houze (1985, 1987a) and others. It is also strongly influenced by the analyses of the 10–11 June 1985 PRE-STORM squall line as described by Rutledge et al. (1988) and Johnson and Hamilton (1988). In the vertical cross section, a general trend of upward motion is seen to begin in the boundary layer near the gust front and extend up through the convective region and to slope more gently into the trailing stratiform cloud at mid to upper levels. Superimposed on the general upflow within the convective region are intense, localized updrafts and downdrafts, associated

³ *Stratiform precipitation* or *stratiform rain* refers to precipitation falling from a stratiform cloud layer. A more vigorous definition is to be found in Houghton (1968) and Houze (1981).

⁴ *Reflectivity* refers to the effective radar reflectivity factor derived from the returned power from a weather radar. It is proportional to the diameter of the precipitation particles raised to the sixth power. Thus, high reflectivities are usually associated with large precipitation particles (large raindrops, hail, etc.). See Battan (1973) for a detailed explanation of the effective radar reflectivity factor.

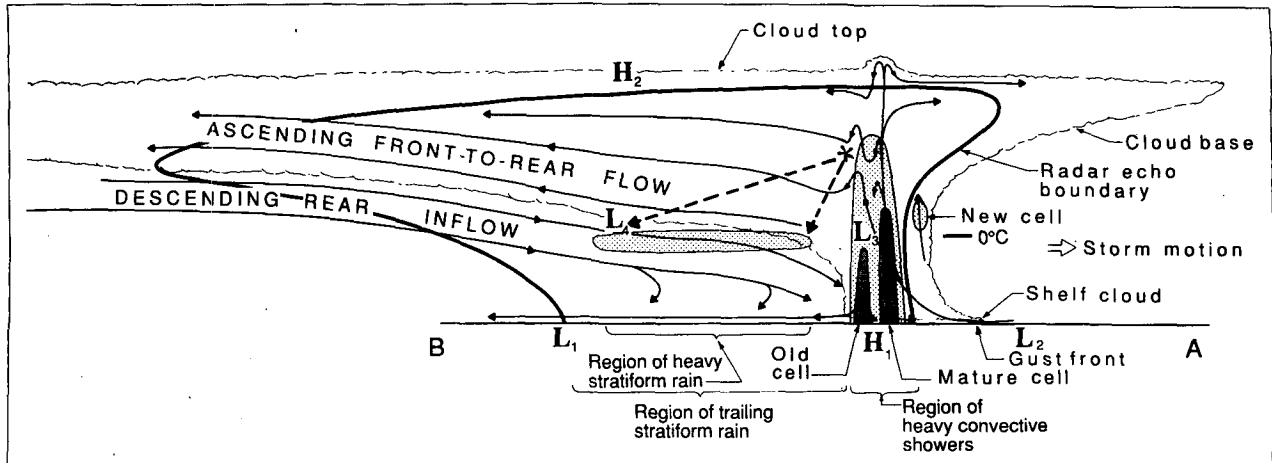


FIG. 1. Conceptual model of a squall line with a trailing stratiform area viewed in a vertical cross section oriented perpendicular to the convective line (i.e., parallel to its motion). See text for further explanation.

with intense cells within the squall line. New convective cells tend to form on or just ahead of the leading edge of the region of heavy convective showers. The first radar echo from a new cell appears aloft, evidently associated with a strong convective updraft. This developing cell is followed by a mature cell, that has a deep, strong reflectivity core and is associated with heavy surface rainfall. The mature cell contains an intense narrow updraft that can penetrate above the top of the broad cirriform cloud shield. This updraft is often followed by a convective-scale downdraft at mid to upper levels.⁵ Following the mature cell is an older cell. Though in a weakening stage, the older cell is also characterized by an updraft core, which is, in turn, followed by another mid- to upper-level convective-scale downdraft. Older cells (not shown), successively farther behind the leading edge of the system, are located at increasingly higher altitudes as they are advected rearward over a layer of dense, subsiding, storm-relative rear inflow. In the heavy rain from the mature and older cells, low-level convective-scale downdrafts, of the type usually associated with "precipitation drag" and evaporation (Byers and Braham 1949), spread out in the boundary layer behind the gust front and toward the rear of the system. Although the cells in figure 1 are shown to be nearly vertical, sometimes they are observed to lean forward or rearward slightly, possibly depending on their stage of development (Rotunno et al. 1988). In tropical convective storms, convective cells tend to have maximum radar reflectivity at low levels, while the maxima tend to occur at higher altitudes in mid-latitude convective storms (Caracena et al. 1979; Zipser and LeMone 1980; Szoke et al. 1986).

The schematic cross section in figure 1 represents

a mature stage in the life of the MCS. At earlier stages, the stratiform rain region (with its accompanying mesoscale circulation pattern and mesoscale precipitation pattern) is not present, and the convective cells are more intense (Leary and Houze 1979; Zipser 1988). Two- and three-dimensional modeling results (e.g., Rotunno et al. 1988; Weisman et al. 1988; Fovell and Ogura 1988) indicate that at first the squall line consists of a line of intense, nearly vertical cells that regenerate somewhat periodically for the first few hours of the storm's existence. As the low-level cold pool associated with precipitation fallout strengthens, the horizontal vorticity associated with it eventually becomes sufficiently strong enough to drive a more slantwise circulation, upon which somewhat weaker but nonetheless significant convective cells continue to form. As the older cells are advected rearward in the sloping flow, the structure indicated in figure 1 evolves. This structure persists between 5 and 10 hours, and is accompanied by large amounts of stratiform rain falling from the trailing region.

The trailing region of stratiform rain is characterized by a marked radar "bright band" (a band of high reflectivity) immediately below the melting level, shown in figure 1 as the horizontal stippled area behind the convective showers, and a layer of subsiding rear-to-front flow, which enters the stratiform rain region just below the trailing stratiform cloud. This storm-relative, rear-to-front flow could be one branch of a midlevel mesoscale vortex in the trailing stratiform rain region (figure 2b) or a horizontally extensive layer that is found throughout the stratiform rain region at mid levels (figure 2a). In either case, as the rear inflow enters the stratiform rain region, it subsides to the level of the bright band and passing through the melting level, finally reaches the back of the convective line at low levels. How much of the rear inflow then enters the convective region and reinforces the convergence at the leading gust front and how much

⁵ This type of mid- to upper-level downdraft has been noted in several recent Doppler-radar studies (Heymsfield and Schotz 1985; Smull and Houze 1987a; Rutledge et al. 1988).

of the rear inflow is blocked and turns parallel to the squall line is unresolved. The strength of the rear inflow appears to vary considerably from storm to storm (Smull and Houze 1987b). The two examples of mid-latitude squall lines presented in sections 4 and 5 have very strong and well-defined rear inflow.

Above the rear inflow, within the stratiform cloud, is a layer of upward-sloping, front-to-rear flow emanating from the upper portions of the convective line. This flow, which contains mesoscale ascending motion, advects ice particles (asterisk) detrained from the convective cells rearward. Since the fallspeed of the ice particles is generally larger than that of the ascending air motion (Rutledge et al. 1988), the ice particles slowly fall as they are carried rearward, growing by vapor deposition in the ascending front-to-rear air flow. Eventually, as the ice particles reach warmer air, they form aggregates. Finally, the aggregates fall through the 0°C level, below which they melt, produce the radar bright band, and produce the region of heavier stratiform rain (figure 1). This view of the stratiform rain (suggested qualitatively by Smull and Houze 1985) is consistent with the numerical calculations of Rutledge and Houze (1987), who showed quantitatively that the amount of stratiform rain that falls is the result of the cooperation of the convective cells, which seed the stratiform region with ice particles, and the mesoscale ascent in the front-to-rear flow, which provides the environment in which the ice particles can continue to grow. The layer between the ascending front-to-rear flow and the descending rear inflow at lower levels in the stratiform region is marked by strong shear, convergence, and vertical and horizontal vorticity. The downward-sloping rear inflow, the front-to-rear flow, and the strong shear separating them can all be identified in real-time single-Doppler-radar displays and are shown especially well in the examples to be discussed in sections 4 and 5.

The low-level reflectivity structure and storm-relative horizontal-airflow patterns associated with the schematic vertical cross section in figure 1 vary from case to case. Schematic drawings of the low-level reflectivity patterns corresponding to the storms to be discussed in sections 4 and 5 are shown in figures 2a and b, respectively. The line AB in each horizontal map indicates the location of the vertical cross section shown in figure 1. Also indicated schematically is the midlevel relative flow, which indicates the presence of a maximum of cyclonic vorticity in the stratiform region, centered in the region of heaviest stratiform rain. In some cases, the vorticity is concentrated along a shear line marking the interface between the front-to-rear and rear-to-front flows (figure 2a). In other cases, the positive vorticity is manifested as a mesoscale vortex (figure 2b). Such vortex

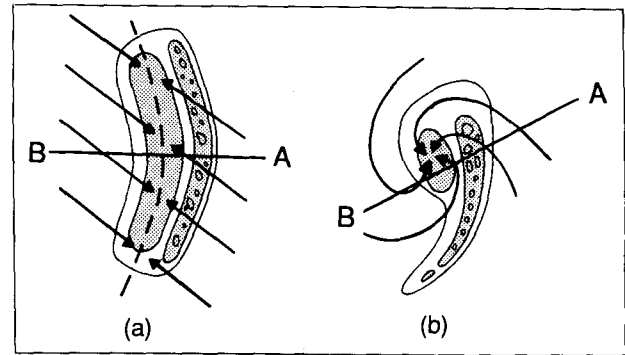


FIG. 2. Conceptual model of a mid-level horizontal cross-section through (a) an approximately two-dimensional squall line, and (b) a squall line with a well-defined mesoscale vortex in the stratiform region. In each case, the midlevel storm-relative flow is superposed on the low-level radar reflectivity. The stippling indicates regions of higher reflectivity.

structure is seen in the observational studies of Houze (1977), Gamache and Houze (1982, 1985), Houze and Rappaport (1984), Smull and Houze (1985), Houze and Wei (1987), and Leary and Rappaport (1987). This type of vortex has also evidently been simulated in a recent numerical study by Zhang and Fritsch (1987). Additionally, the midlevel relative flow may evolve from one type to another, with an initially sheared flow (figure 2a) becoming increasingly curved and eventually developing a closed vortex (figure 2b) or breaking down into multiple vortices (Stirling and Wakimoto 1988).

The stratiform precipitation is eroded by the intrusion of the midlevel rear inflow. This erosion can be manifested as a small "notch" in the low-level reflectivity at the back of the stratiform rain region (Smull and Houze 1985), or, when a strong vortex is present, the southern part of the stratiform rain region can be practically missing, as in figure 2b.

The pressure field associated with the mesoscale system is marked by several characteristic mesolows and mesohighs (indicated by L and H in figure 1). A "wake" low (L_1) occurs at the surface at the back edge of the stratiform rain, in association with warming due to unsaturated descent, and a mesohigh (H_1) occurs below the convective region (Fujita 1955; Pedgley 1962; Johnson and Nicholls 1983; Smull and Houze 1985; Johnson and Hamilton 1988). Also, a weak mesolow (L_2), associated with warming by compensating downward motion is often noted ahead of the convective line at the surface (Hoxit et al. 1976; Fritsch and Chappell 1980). In the midtroposphere a small, apparently hydrostatic mesolow (L_3) is located below the primary sloping buoyant convective updraft (LeMone 1983). Farther to the rear, in the vicinity of the melting layer or just above is another mesolow (L_4) that is larger in scale. This mesolow has been indicated by modeling studies (especially by Brown 1979) and in the geopotential-height data associated with the 10–11 June 1985 PRE-STORM squall line

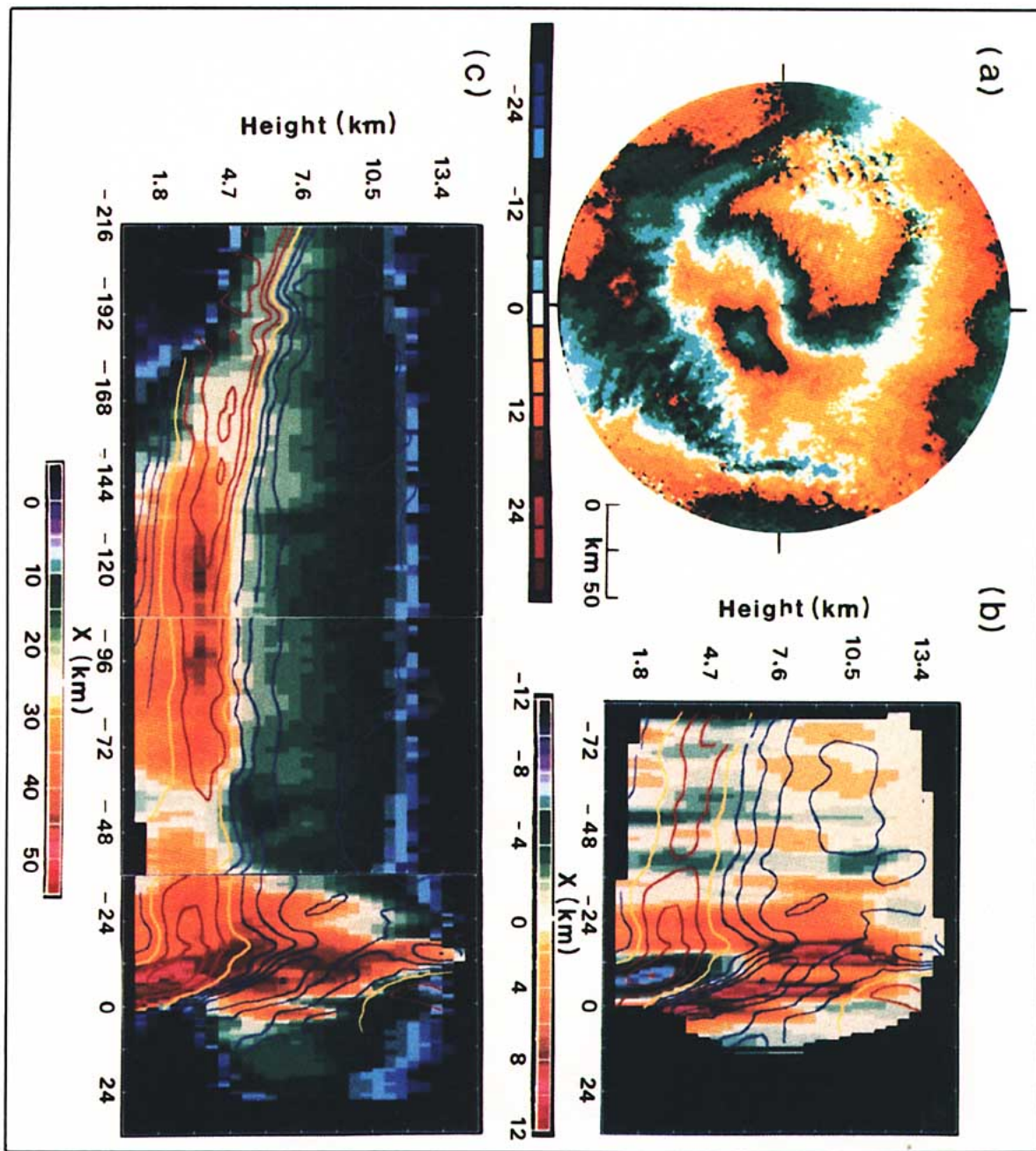


FIG. 4. Doppler-radar display and analyses of the 10-11 June 1985 storm: (a) Raw (folded) radial velocity storm taken from the 3.6° Ver-CPPI CP scan at 0350 UTC. (b) Vertical cross section taken from the 10-11 June Doppler analysis illustrating the vertical velocity (m s⁻¹, color background) in the convection region. Overlaid on the vertical velocity are contours of the storm-relative horizontal wind component in the plane of the cross section (i.e., normal to the squall line). The contours are spaced every 5 m s⁻¹ with red indicating positive values (i.e., flow from left to right) and blue for negative values. (c) Composite vertical cross section of radar reflectivity (dBZ) taken from the dual-Doppler analyses at 0350 and 0356 UTC. The discontinuity of x = 36 km corresponds to the boundary between the two analyses periods. The overlaid contours are the same as in panel b.

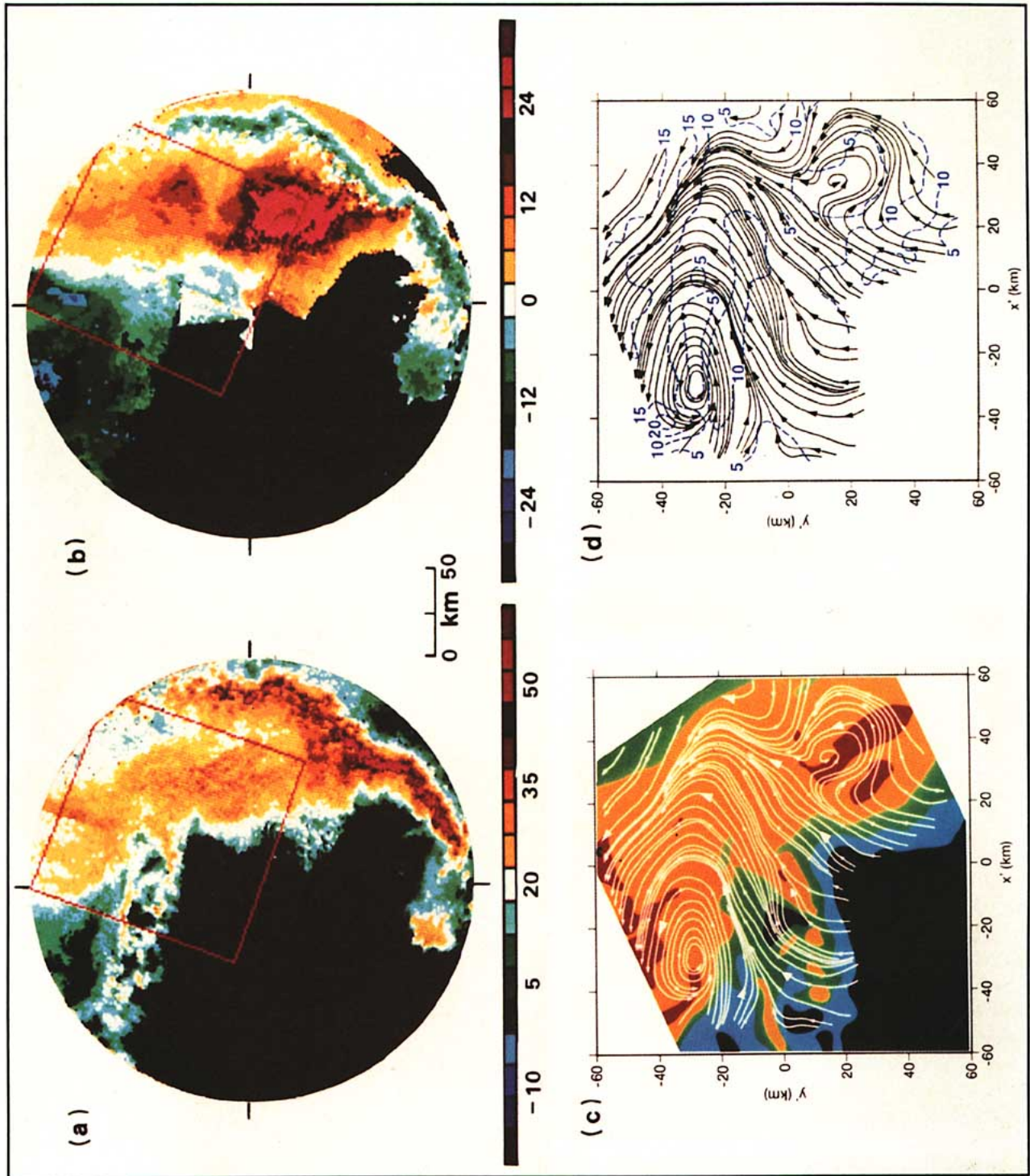


FIG. 5. Doppler-radar displays and analyses of the 28 May 1985 storm: (a) Radar reflectivity (dBZ) taken from the 2.0° PPI CP4 scan at 1308 UTC. The red box indicates the region in which the dual-Doppler analysis has been performed. The black tick marks are spaced every 90° with north at the top. (b) Edited (unfolded) radial velocity ($m s^{-1}$) field corresponding to panel a. (c) The 3.4 km MSL streamline-reflectivity display from the dual-Doppler analyses at 1308 UTC. The streamlines, in white, are overlaid on the reflectivity field. Reflectivity levels are: <5 dBZ, black; 5–15 dBZ, blue; 15–25 dBZ, green; 25–35 dBZ, orange; and 35–45 dBZ, red. The box is oriented such that the positive x' -axis points toward 120° from north (i.e., toward the east-southeast, so that the sides of this box are parallel to the red box in (a) and (b)). (d) The 3.4 km MSL streamline-isotach analysis corresponding to (c). The streamlines are in black and isotachs, spaced every 5 $m s^{-1}$ apart, are in blue. The orientation of this box is the same as in (c).

(Johnson and Gallus 1988). A mesohigh at upper levels (H_2) atop the entire mesoscale cloud system is a widely recognized feature that becomes particularly well marked in the case of mesoscale convective complexes (Fritsch and Maddox 1981a, b; Maddox et al. 1981).

It should be noted that the conceptual models presented in figures 1 and 2 are idealized and few cases exhibit all of the features shown. For example, in some storms the rear inflow is strong while in others it is weak (Smull and Houze 1987b), and the mesoscale vortex is better defined in some cases than others.

3. The Doppler radar data and methods of analysis

Doppler weather radar measures the returned power from targets in a discrete region of the atmosphere (the "sampling volume") and the mean velocity component of those targets along the radar beam (the "radial velocity"). The patterns we present below are composed of "edited" radial-velocity and reflectivity (derived from the returned power) data. The velocity fields have had samples with low returned power removed and, with one exception, have been "unfolded." Pulsed Doppler radars such as the NCAR 5-cm radars used in this study are characterized by a maximum unambiguously detectable radial velocity (V_{\max}).⁶ For PRE-STORM, V_{\max} was $\pm 15.37 \text{ m s}^{-1}$ for CP-3 and $\pm 15.24 \text{ m s}^{-1}$ for CP-4. Because of frequent high-wind situations encountered during the field program, velocity "folds," i.e., actual radial velocities falling outside this range, were rather common. Such folds must be identified and corrected for (unfolded) by adding or subtracting the correct number of Nyquist intervals ($2|V_{\max}|$) to the radial-velocity data obtained from the NCAR Doppler radars. Presentation of unfolded velocity data makes the interpretation of the fields more straightforward. Range folding and attenuation also presented problems at times in storms with high reflectivities. The NEXRAD radars will have a 10-cm wave length, hence alleviating velocity and range folding problems, as well as attenuation by strong convective cores. In addition, NEXRAD radars will employ real-time algorithms to present unfolded wind displays. Hence, the unfolded displays shown in this paper simulate patterns as they would likely appear on a NEXRAD radar.

⁶ $V_{\max} = \pm P\lambda/4$ where P is the pulse repetition frequency (in Hz); $P = 1111 \text{ Hz}$ for the PRE-STORM Kansas radar pair) and λ is the radar wavelength ($\lambda = 0.0545 \text{ m}$ for CP-3; $\lambda = 0.0549 \text{ m}$ for CP-4).

Color photographs of unfolded velocity patterns for the first of the two PRE-STORM squall lines that will be discussed (10–11 June 1985) are shown on the cover. The raw (or folded) version of the radial-velocity pattern, whose unfolded version is seen in the lower right cover photograph, is shown in figure 4a. In the unfolded pattern on the cover, the white area corresponds to an area of essentially zero radial velocity. Either the wind speed in the white area was truly zero or the wind direction in the white area was normal to the radar's beam. The dark blue feature to the west-northwest of the radar, which is located at the center of the display, is correctly indicated as approaching the radar at a maximum speed $> 30 \text{ m s}^{-1}$. Because this velocity exceeds $|V_{\max}|$ in magnitude, it is aliased in the raw (folded) velocity pattern as only slightly greater than 0 m s^{-1} and hence appears as a green core surrounded by a ring of white (figure 4a). Velocities were unfolded by assuming that the white band closest to the center of the PPI (the location of the radar) was the true zero radial-velocity region.⁷ Then, proceeding radially outward from the white band, a continuous velocity field was produced by adding or subtracting the correct number of Nyquist intervals that would minimize the radial shear. This procedure usually led to a velocity field free of artificial discontinuities and labeled in accordance with the color bar seen in the cover photographs. (For further discussion of the unfolding of Doppler-velocity fields see Baynton et al. 1977.)

In sections 4 and 5, we show some results obtained from dual-Doppler analyses of the velocity fields detected simultaneously by the CP-3 and CP-4 radars. Although multiple-Doppler data are not likely to be routinely available in an operational NEXRAD setting, we present these dual-Doppler analyses to confirm and indicate more clearly certain features of the conceptual models presented in figures 1 and 2. Specifically, the dual-Doppler analyses allow the convective cell structure sketched in figure 1 to be seen (section 4) and the vortex structure indicated in figure 2b to be documented in a particular case (section 5). The steps taken in performing the dual-Doppler analyses are outlined in the appendix.

4. The 10–11 June 1985 PRE-STORM squall line

This storm has been the subject of several PRE-STORM research investigations.⁸ For a description of the storm's

⁷ The assumption was verified by measurements of the winds at the radar sight and by comparison of the Doppler-radar data with winds measured by aircraft and rawinsondes.

history, the reader is referred to Rutledge et al. (1988). The low-level PPI reflectivity and unfolded-velocity patterns from the CP-4 radar at 0345 UTC 11 June (0.2° elevation) are shown in the upper left and upper right portions of the cover. At this time, the storm was in a mature phase. The stratiform region was well defined, with a band-like echo (~30 dBZ) marking its most intense area (cover, upper left). A weak-echo "gap" or "transition zone" (Smull and Houze 1985) separated the most intense portion of the stratiform region from the convective line and reflectivities exceeded 40 dBZ in the convective line.

An isolated convective cell, although quite shallow, was present along the rear portion of the stratiform rain area and was likely associated with convergence into a wake low-pressure feature (Johnson and Hamilton 1988). The radial-velocity pattern (cover, upper right) indicates diffluent flow at low levels (note the V-shape of the white [zero radial-velocity] band) associated with outflow from a well-defined mesoscale downdraft (Rutledge et al. 1988). The flow switches from north-northwesterly east of the radar to northeasterly west of CP-4 as indicated by the zero-velocity band.

To aid in comparing the observed structure of this storm to that shown in the conceptual model (figure 1), a plot of the height of the radar beam above the ground for the 0.2°, 2.0°, and 3.6° elevation angles is shown in figure 3. At 0.2°, the radar beam is essentially at a "constant" altitude. The center of the beam goes from zero to slightly higher than 1 km above the ground through the 133 km radial range of the radar. However, at 3.6°, the center of the radar beam goes from zero to about 9 km above the ground over the same radial distance. Thus, the vertical structure of the reflectivity and unfolded radial velocity from CP-4 at 0350 UTC are indicated by the 3.6° elevation angle PPI (cover, lower left, and lower right). The reflectivity display (cover, lower left) indicates the pronounced stratiform nature of the echo behind the convective line. The circular band of high reflectivities at a slant range of approximately 50 km clearly defines the radar bright band located immediately below the melting level. The range of the bright band at this elevation angle indicates (according to figure 3) an approximate height of 3.3 km AGL (above ground level) for the melting level. Convective cells along the squall line are evident in a band running from east-northeast to south-southeast of the radar in this display. The maximum reflectivities there were 50 dBZ.

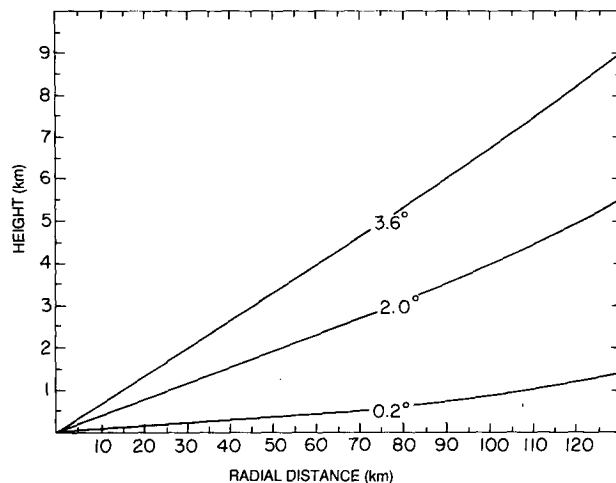


FIG. 3. Height of center of radar beam above ground level assuming a spherical earth and a standard atmospheric index of refraction. The 0.2° and 3.6° elevation angles correspond to displays for the 10–11 June 1985 storm while the 2.0° elevation angle is for the 28 May 1985 storm.

The unfolded velocity pattern at 0350 UTC (cover, lower right) shows two important mesoscale-flow features consistent with the conceptual model (figure 1). The first is the strong rear-inflow jet, which is indicated by the enclosed dark blue and red regions in the radial-velocity data, denoting the presence of intense northwesterly flow above the radar. Speeds within the rear inflow were $>30 \text{ m s}^{-1}$ relative to the ground. Since the storm was moving toward the southeast at 14 m s^{-1} , it follows that the rear-inflow jet had relative speeds of $>16 \text{ m s}^{-1}$ in the trailing stratiform rain region. The difference in the peak radial velocity between the upwind (dark blue) and downwind (red) velocity cores indicates that the speed of the rear inflow decreased toward the back of the convective line. This decrease in speed helps to explain the apparent decrease in the size of the velocity feature seen in the PPI display. However, results from the dual-Doppler analysis (figure 4c) show that the depth of the rear inflow also decreased slightly toward the rear of the convective line. Another aspect of the rear inflow that can be seen in the PPI display is that the core of the jet appeared at a smaller slant range downwind than it did upwind of the radar. Thus the rear-inflow jet tilted with height, sloping downward towards the southeast with a slope of 1 km in the vertical to 40 km in the horizontal. Upwind, the core is at a height of 4.5 km above ground compared to only 2.0 km downwind. At the top of the rear inflow, a sharp wind shift occurred as the wind backed from $300^\circ/25 \text{ m s}^{-1}$ to $240^\circ/10 \text{ m s}^{-1}$. This strong wind shift constituted a layer of shear instability.

The second important mesoscale feature in the unfolded velocity pattern (cover, lower right) is a front-to-rear jet, seen in the pattern of the radial velocity

⁹ Augustine and Zipser 1987; Smull and Houze 1987b; Rutledge et al. 1988; Johnson and Hamilton 1988; Rutledge and MacGorman 1988; Johnson and Gallus 1988; Biggerstaff et al. 1988.

near the convective line. The flow above the strong shear layer was directed front-to-rear relative to the storm (as indicated by the conceptual model in figure 1). Indications of this front-to-rear storm-relative flow, which is most intense immediately behind the convective cells, are seen in this PPI display as a band of negative radial velocities (green, indicating flow toward the radar) southeast of the radar at slant ranges between 65 and 95 km (heights of 4.4 to 6.5 km AGL). Ground-relative winds approach maxima of 13 m s^{-1} ; relative to the storm they are rearward at 27 m s^{-1} . As noted in the discussion of the fallout of snow represented in the conceptual model (figure 1), this front-to-rear flow is important to the horizontal transfer of momentum and condensate into the stratiform region. At slant ranges beyond 100 km east of the radar, the flow reverses in association with upper-level divergent outflow from the convective cells.

As noted earlier, the wind shift between the rear inflow and the front-to-rear flow constituted a layer of shear instability. The shear at the interface between the two mesoscale flows was so extreme that the Richardson number in this region was about 0.3, which is just above the critical threshold of 0.25 required for the onset of Kelvin–Helmholtz instability (Taylor 1931; Goldstein 1931), but is well below the threshold of 1.0 required for the continuation of Kelvin–Helmholtz waves once the waves have begun (Wallace and Hobbs 1977).⁹ Evidence of Kelvin–Helmholtz waves is found in this shear layer. Looking at the upper left quadrant of the raw (folded) radial-velocity data (figure 4a), the waves appear as a series of very thin, short bands of green (negative) raw velocities adjacent to yellow (positive) raw velocities. These waves are also evident in the unfolded radial-velocity data (cover, lower right) but the color contrast (green adjacent to dark blue) for most of the waves is not as great after correcting for the fold in the raw velocity data. Reports of moderate turbulence from the NOAA WP-3D aircraft, which flew this region of the storm, provides further evidence that the shear instability produced Kelvin–Helmholtz waves.

The vertical structure of the 10–11 June storm is illustrated in cross-sectional form in figures 4b and 4c. These figures were derived by dual-Doppler synthesis of data from the two NCAR radars. Except for the vertical air-motion pattern included in figure 4b, the fields depicted are similar to those that would be detected by a single-Doppler radar such as NEXRAD. Smull and Houze (1987b) and Rutledge et al. (1988)

present examples of single-Doppler cross sections from the 10–11 June storm that are very similar to figure 4c.

The vertical cross section normal to the convective line in figure 4c is pieced together from dual-Doppler analyses of data taken at two different times (0144 and 0350 UTC). This provides a representative cross section through the entire storm, which can be compared to the conceptual model in figure 1. The color background in figure 4c is the radar reflectivity and it shows multicellular development similar to that depicted in the conceptual model. The overlaid color contours in figures 4b and 4c indicate the storm-relative horizontal flow normal to the squall line. The rear inflow entered the stratiform rain region from the back edge at an altitude of about 7.5 km above mean sea level (MSL).¹⁰ The layer of rear inflow was located at successively lower levels from back to front of the storm system. This layer dropped sharply at the back edge of the stratiform rain region and then more gently through the stratiform region, where it was centered on the radar-reflectivity bright band ($\approx 3.7 \text{ km MSL}$). The strong vertical gradient of the contours at the back edge of the storm ($x < -156$) corresponds to the region of Kelvin–Helmholtz instability shown in figure 4a. Where the layer of rear inflow sloped downward through the stratiform rain region, the speed of the system-relative wind decreased in magnitude from more than 15 m s^{-1} at the back edge to roughly 5 m s^{-1} close to the transition zone. From there the layer of rear inflow entered the back edge of the intense convective region. In the convective region the rear inflow descended sharply and increased in speed to roughly 15 m s^{-1} .

The location at which the rear inflow apparently descended and increased in speed corresponds to the location of an intense convective-scale downdraft shown in figure 4b. Moreover, the strong convective-scale downdraft is seen to correspond to the radar-reflectivity maximum at the low levels (cf. figures 4b and 4c between $x = 0$ and -15 km). Ahead of and above this downdraft, three convective-scale maxima of updraft intensity are seen at a series of successively higher levels—lowest at the leading edge ($x = 0 \text{ km}$) and becoming higher toward the rear of the convective region ($x = -18 \text{ km}$). The multicellular pattern of updraft cores stairstepping upward across the squall line was noted previously by Smull and Houze (1987a) and Biggerstaff et al. (1988) and is depicted in figure 1.

Behind the convective region, in the transition zone and stratiform rain region, the cores of vertical drafts

⁹ The Richardson number, Ri , is given by $Ri = N^2/S^2$ where N is the Brunt–Väisälä frequency and S is the vertical shear of the horizontal wind. A sounding taken from Russell, Kansas at 0250 UTC on 11 June 1985 was used to determine N . Dual-Doppler-derived horizontal winds were used to determine S .

¹⁰ The height of the radar from which the PPIs were taken was 438 MSL. To obtain heights in AGL, add 438 m to heights given in MSL.

decreased in intensity and broadened in width. The layer of front-to-rear flow aloft was dominated by upward vertical motion while the rear flow layer at lower altitudes was dominated by downward motion. As depicted in the conceptual model, the front-to-rear flow was observed to intensify as it passed through the convective region.

5. The 28 May 1985 PRE-STORM squall line

The 10–11 June radar data do not provide an example of the cyclonic mesoscale vortex seen in the stratiform–rain region of the schematic model (figure 2b). However, several other cases observed in PRE-STORM provide examples of these mesovortices. To illustrate this feature, we include the case of 28 May 1985 (figure 5). The reflectivity pattern taken at an elevation angle of 2.0° (figure 5a) indicates a curved line of leading convection, which was more intense toward the south and preceded a trailing stratiform rain region, which increased in width towards the north.

The accompanying radial-velocity pattern is shown in figure 5b. The rear-inflow jet (red core, ground-relative speed of 26 m s^{-1} ; system-relative speed of 10 m s^{-1}) and intense front-to-rear flow (denoted again by the thin band of negative [green] velocities near the convective line) were clearly present. In this case, the rear-inflow jet was the southern branch of a mesoscale cyclonic vortex (as in figure 2b). This mesovortex is confirmed and further illustrated by a streamline analysis of one of the dual-Doppler–derived velocity patterns obtained for this storm (figure 5c). The vortex is shown at the 3.4 km level, where it is seen to have had horizontal dimensions of at least 100 km. The pattern exhibited a closed cyclonic circulation at the rear of the stratiform region (in agreement with the conceptual model shown in figure 2b). This circulation was observed to extend from the lowest observation level (1.4 km) up to approximately 8 km. A secondary cyclonic circulation (considerably smaller in horizontal and vertical scale) is also seen in the lower right-hand portion of figure 5c. Figure 5c also shows the relationship between the streamline pattern and the reflectivity pattern at the 3.4 km level. Cyclonic curvature is suggested in the reflectivity pattern near the large vortex (see the hook-shaped 35 dbZ contour in the top portion of figure 5c). Similar reflectivity structure in the dissipating stratiform region of an Oklahoma squall line was observed by Smull and Houze (1985) who attributed its development to the presence of cyclonic midlevel vortices. Velocity patterns from a single Doppler-radar, consistent with such vortices in a MCS observed during

COMEX (the Cooperative Huntsville Meteorological Experiment) have recently been presented by Stirling and Wakimoto (1988). The analysis presented in figure 5 marks the first confirmation provided by dual-Doppler measurements which, unlike single-Doppler measurements, yields both components of the horizontal wind and displays the vortex on a constant altitude surface rather than on a tilted PPI surface. Several narrow bands of enhanced reflectivity extending into the vortex region from the northwest (cf. figure 5a) appear to be related to confluent zones in the rear inflow (figure 5c). The isotach analysis at this level (figure 5d) indicated speeds ranging from 5 to 20 m s^{-1} around the vortex with strong convergence behind the vortex. Airflow at this level was typically 10 m s^{-1} with divergence in the front-to-rear branch of the vortex and convergence in the rear inflow branch. Rainbands spiraling into a midlevel cyclonic vortex (identified by network rawinsonde data) were also noted by Leary and Rappaport (1987) in a detailed reflectivity analysis of the trailing stratiform region of a mesoscale convective system.

6. Conclusions

We have illustrated that PPI displays from a single Doppler radar can indicate several important features of the mesoscale circulations in mesoscale convective systems in real time. In particular, the descending rear-inflow jet, the ascending front-to-rear flow lying just above and low-level mesoscale diffluence in the stratiform rain region, indicating the presence of the mesoscale downdraft, are all routinely clearly evident in Doppler displays from a single radar. The characteristic patterns associated with these features should be especially useful to meteorologists at future NEXRAD radar installations in the interpretation of mesoscale storm structure and behavior. The further ability of the dual-Doppler syntheses to show the structure of the vertical drafts and to show the rear inflow and front-to-rear flow in more detail, allowing those features to be related to the characteristic mesoscale vortex in the stratiform region, indicates that multiple-Doppler syntheses will contribute strongly to the research objectives of the National STORM Program.

Acknowledgments. The data presented in this paper were collected by the Field Observing Facility of NCAR. The color-display software for the multiple-Doppler-radar analyses was developed at the University of Washington by Dr. Dean D. Churchill. A portion of the computing support was provided by NCAR. Kay Dewar and Jim Adams assisted in layout and drafting the figures. This research was supported by National Science Foundation Grants ATM8413546, ATM8521403, and ATM8602411.

Appendix. Steps Taken in Performing the Dual-Doppler Analysis

First the Doppler data from both the CP-3 and CP-4 radars were edited and unfolded using versions of the NCAR Research Data Support System (RDSS) software, which was transferred to PRIME and Masscomp (UNIX) computer systems at the University of Washington and to a VAX computer at Colorado State University. The radar data were then interpolated to a common Cartesian grid using a grid spacing of 1.5 km in the horizontal and 0.5 km in the vertical by the sorted position radar interpolation (SPRINT) software developed at NCAR (Mohr et al. 1979). The horizontal winds were then derived from a two-radar synthesis (which assumes that the vertical velocity is zero) by means of the Cartesian editing and display of radar data under interactive control (CEDRIC) software developed at NCAR by Mohr and Miller (1983). The interpolation and synthesis was accomplished with versions of SPRINT and CEDRIC operating on the University of Washington Cloud Physics Group's Harris Computer.

Precipitation-particle fallspeeds were removed from the horizontal wind estimates using a reflectivity-weighted fallspeed. Divergence was then calculated. The vertical velocity was obtained by integrating the anelastic continuity equation downward using a boundary condition between 0.10 and 0.25 m s⁻¹ in the convective region and zero elsewhere. A more complete discussion of the choice of the boundary condition was presented by Biggerstaff et al. (1988). Corrections for the vertical velocity were then made to the horizontal winds from which a new estimate of divergence and vertical velocity were obtained. This procedure was repeated until the mean of the absolute value of the change in horizontal wind components at each level from one iteration to the next was less than 0.1 m s.

References

- Augustine, J. A., and E. J. Zipser. 1987. The use of wind profilers in a mesoscale experiment. *Bull. Amer. Meteor. Soc.* **68**: 4–17.
- Battan, L. J. 1973. *Radar observation of the atmosphere*. Chicago: University of Chicago Press.
- Baynton, H. W., R. J. Serafin, C. I. Frush, G. R. Gray, P. V. Hobbs, R. A. Houze, Jr., and J. D. Locatelli. 1977. Real-time wind measurement in extratropical cyclones using Doppler radar. *J. Appl. Meteor.*, **16**: 1022–1028.
- Biggerstaff, M. I., R. A. Houze Jr., and S. A. Rutledge. 1988. Vertical drafts in the convective regions of Mesoscale Convective Systems in Kansas. Preprints, Tenth International Cloud Physics Conference, Bad Homburg, 15–20 August 1988. pp. 705–707. Offenbach am Main: Deutscher Wetterdienst.
- Brown, J. M. 1979. Mesoscale unsaturated downdrafts driven by rainfall evaporation: A numerical study. *J. Atmos. Sci.* **36**: 313–338.
- Byers, H. R., and R. R. Braham. 1949. *The Thunderstorm*. Washington, DC: U.S. Printing Office.
- Caracena, F., R. A. Maddox, L. R. Hoxit, and C. F. Chappell. 1979. Meso-analysis of the Big Thompson Storm. *Mon. Wea. Rev.* **107**: 1–17.
- Cunning, J. B. 1986. The Oklahoma-Kansas preliminary regional experiment for STORM-Central. *Bull. Amer. Meteor. Soc.* **67**: 1478–1486.
- Foyell, R. G., and Y. Ogura. 1988. Numerical simulation of a midlatitude squall line in two dimensions. *J. Atmos. Sci.* **45**: 3846–3879.
- Fritsch, J. M., and C. F. Chappell. 1980. Numerical prediction of convectively driven mesoscale pressure systems. II. Mesoscale model. *J. Atmos. Sci.* **37**: 1734–1762.
- Fritsch, J. M., and R. A. Maddox. 1981a. Convectively driven mesoscale weather systems aloft. Part I: Observations. *J. Appl. Meteor.* **20**: 9–19.
- , and ———. 1981b. Convectively driven mesoscale weather systems aloft. Part II: Numerical simulations. *J. Appl. Meteor.* **20**: 20–26.
- Fritsch, J. M., R. J. Kane, and C. R. Chelius. 1986. The contribution of mesoscale convective weather systems to the warm-season precipitation in the United States. *J. Climate and Appl. Meteor.* **25**: 1333–1345.
- Fujita, T. T. 1955. Results of detailed synoptic studies of squall lines. *Tellus*. **7**: 405–436.
- Gamache, J. F., and R. A. Houze, Jr. 1982. Mesoscale air motions associated with a tropical squall line. *Mon. Wea. Rev.* **110**: 118–135.
- , and ———. 1985. Further analysis of the composite wind and thermodynamic structure of the 12 September GATE squall line. *Mon. Wea. Rev.* **113**: 1241–1259.
- Goldstein, S. 1931. On the stability of superposed streams of fluids of different densities. *Proc. Roy. Soc. A.* **132**: 524–548.
- Hamilton, R. A., and J. W. Archbold. 1945. Meteorology of Nigeria and adjacent territory. *Quart. J. Roy. Meteor. Soc.* **71**: 231–265.
- Heymselfield, G. M., and S. Schotz. 1985. Structure and evolution of a severe squall line over Oklahoma. *Mon. Wea. Rev.* **113**: 1563–1589.
- Houghton, H. G. 1968. On precipitation mechanisms and their artificial modification. *J. Appl. Meteor.* **7**: 851–859.
- Houze, R. A., Jr. 1977. Structure and dynamics of a tropical squall-line system. *Mon. Wea. Rev.* **105**: 1540–1567.
- . 1981. Structures of atmospheric precipitation systems: A global survey. *Radio Sci.* **16**: 671–689.
- Houze, R. A., Jr., and E. N. Rappaport. 1984. Air motions and precipitation structure of an early summer squall line over the eastern tropical Atlantic. *J. Atmos. Sci.* **41**: 553–574.
- Houze, R. A., Jr., and T. Wei, 1987. The GATE squall line of 9–10 August 1974. *Advances in Atmospheric Sciences* **4**: 85–92.
- Hoxit, L. R., C. F. Chappell, and J. M. Fritsch. 1976. Formation of mesolows or pressure troughs in advance of cumulonimbus clouds. *Mon. Wea. Rev.* **104**: 1419–1428.
- Johnson, R. H., and W. G. Gallus. 1988. The wake structure of an intense midlatitude squall line in OK PRE-STORM. Eighth Conf. on Numerical Weather Prediction and 15th Conf. on Severe Local Storms. AMS Reprint, pp. 229–232. Boston: American Meteorological Society.
- Johnson, R. H., and P. J. Hamilton. 1988. The relationship of surface pressure features to the precipitation and air flow structure of an intense midlatitude squall line. *Mon. Wea. Rev.* **116**: 1444–1472.
- Johnson, R. H., and M. E. Nicholls. 1983. A composite analysis of the boundary layer accompanying a tropical squall line. *Mon. Wea. Rev.* **111**: 308–319.
- Leary, C. A. and R. A. Houze, Jr. 1979. The structure and evolution of convection in a tropical cloud cluster. *J. Atmos. Sci.* **36**: 437–457.
- Leary, C. A., and E. N. Rappaport. 1987. The life cycle and internal structure of a mesoscale convective complex. *Mon. Wea. Rev.* **115**: 1503–1527.
- LeMone, M. A. 1983. Momentum transport by a line of cumulonimbus. *J. Atmos. Sci.* **40**: 1815–1834.
- Maddox, R. A. 1980. An objective technique for separating macroscale and mesoscale features in meteorological data. *Mon. Wea. Rev.* **108**: 1108–1121.
- Maddox, R. A., D. J. Perkey, and J. M. Fritsch. 1981. Evolution of upper tropospheric features during the development of a mesoscale convective complex. *J. Atmos. Sci.* **38**: 1664–1674.
- Matejka, T. J., and P. V. Hobbs. 1981. The use of a single Doppler

- radar in short-range forecasting and real-time analysis of extratropical cyclones. Nowcasting: Mesoscale observations and short-range prediction. Proceedings, International Symposium of International Association of Meteorology and Atmospheric Physics, Hamburg, 25–28 August 1981. Paris: European Space Agency. 177–182.
- Mohr, C. G., and R. L. Vaughn. 1979. An economical procedure for Cartesian interpolation and display of reflectivity factor data in three-dimensional space. *J. Appl. Meteor.* **18**: 661–670.
- Mohr, C. G., and L. J. Miller. 1983. CEDRIC—A software package for Cartesian space editing, synthesis and display of radar fields under interactive control. 21st Conf. on Radar Meteor., Edmonton, Alta., Canada. Boston: American Meteorological Society. AMS Reprints, pp. 559–574.
- NCAR. 1984. The National STORM Program: STORM-Central Phase. Prepared by the National Center for Atmospheric Research, Boulder, Colorado, in consultation with the Interagency Team for STORM-Central. Boulder: NCAR.
- Newton, C. W. 1950. Structure and mechanism of the prefrontal squall line. *J. Meteor.* **7**: 210–222.
- Pedgley, D. E. 1962. A meso-synoptic analysis of the thunderstorms on 28 August 1958. *Brit. Meteor. Off., Geophys. Mem.*, No. 106. London: Her Majesty's Stationery Office.
- Ray, P. S. and D. P. Jorgensen. 1988. Uncertainties associated with combining airborne and ground-based Doppler radar data. *J. Atmos. and Oceanic Tech.* **5**: 177–196.
- Ray, P. S., and K. Colbert, eds. 1982. *Proceedings of the NEXRAD Doppler radar symposium/workshop*. Cooperative Institute for Mesoscale Meteorological Studies. Norman: University of Oklahoma.
- Ray, P. S., C. L. Ziegler, W. Bumgarner, and R. J. Serafin. 1980. Single- and multiple-Doppler radar observations of tornadic storms. *Mon. Wea. Rev.* **108**: 1607–1625.
- Rotunno, R., J. B. Klemp, and M. L. Weisman. 1988. A theory for strong, long lived squall lines. *J. Atmos. Sci.* **45**: 463–485.
- Rutledge, S. A. and R. A. Houze, Jr. 1987. A diagnostic modeling study of the trailing stratiform region of a midlatitude squall line. *J. Atmos. Sci.* **44**: 2640–2656.
- Rutledge, S. A., and D. R. MacGorman. 1988. Cloud-to ground lightning in the 10–11 June 1985 mesoscale convective system observed during O.K. PRE-STORM. *Mon. Wea. Rev.* **116**: 1393–1408.
- Rutledge, S. A., R. A. Houze, Jr., M. I. Biggerstaff, and T. Matejka. 1988. The Oklahoma-Kansas mesoscale convective system of 10–11 June 1985: Precipitation structure and single-Doppler radar analysis. *Mon. Wea. Rev.* **116**: 1409–1430.
- Smull, B. F., and R. A. Houze, Jr. 1985. A midlatitude squall line with a trailing region of stratiform rain: radar and satellite observations. *Mon. Wea. Rev.* **113**: 117–133.
- and ——— 1987a. Dual-Doppler radar analysis of a midlatitude squall line with a trailing region of stratiform rain. *J. Atmos. Sci.* **44**: 2128–2148.
- Smull, B. F., and R. A. Houze, Jr. 1987b. Rear inflow in squall lines with trailing stratiform precipitation. *Mon. Wea. Rev.* **115**: 2869–2889.
- Stirling, J., and R. M. Wakimoto. 1988. Mesoscale vortices in the stratiform region of a decaying midlatitude squall line. *Mon. Wea. Rev.* **117**: 452–458.
- Szoke, E. J., E. J. Zipser and D. P. Jorgensen. 1986. A radar study of convective cells in mesoscale systems in GATE. Part I: Vertical profile statistics and comparison with hurricanes. *J. Atmos. Sci.* **43**: 182–197.
- Taylor, G. I. 1931. Effect of variation in density on the stability of superposed streams of fluid. *Proc. Roy. Soc. A* **132**: 499–523.
- Wallace, J. M., and P. V. Hobbs. 1977. *Atmospheric Science: An Introductory Survey*. New York: Academic Press.
- Weisman, M. L., J. B. Klemp, and R. Rotunno. 1988. The structure and evolution of numerically simulated squall lines. *J. Atmos. Sci.* **45**: 1990–2013.
- Wilson, J., R. Carbone, H. Baynton and R. Serafin. 1980. Operational application of meteorological Doppler radar. *Bull. Amer. Meteor. Soc.* **61**: 1154–1168.
- Zhang, D. L., and J. M. Fritsch. 1987. Numerical simulation of the meso-b scale structure and evolution of the 1977 Johnstown flood. Part II: Inertially stable warm-core vortex and the mesoscale convective complex. *J. Atmos. Sci.* **44**: 2593–2612.
- Zipser, E. J. 1969. The role of organized unsaturated convective downdrafts in the structure and rapid decay of an equatorial disturbance. *J. Appl. Meteor.* **8**: 799–814.
- 1977. Mesoscale and convective-scale downdrafts as distinct components of squall-line circulation. *Mon. Wea. Rev.* **105**: 1568–1589.
- 1988. The evolution of mesoscale convective systems: Evidence from radar and satellite observations. Proceedings, International Symposium on Tropical Precipitation Measurements. Tokyo, Japan. Hampton, VA: Science & Technology Co. In press.
- Zipser, E. J., and M. A. LeMone. 1980. Cumulonimbus vertical velocity events in GATE. Part II: Synthesis and model core structure. *J. Atmos. Sci.* **37**: 2458–2469. ●